Heliyon 11 (2025) e41646

Contents lists available at ScienceDirect

Heliyon

journal homepage: www.cell.com/heliyon

Research article

TEMPO-oxidized cellulose fiber from spent coffee ground: Studying their properties as a function of particle size

Hooriyeh Rahmani Khoshk, Marzieh Moeenfard *

Department of Food Science and Technology, Faculty of Agriculture, Ferdowsi University of Mashhad, Mashhad, Iran

ARTICLE INFO

Keywords:
TEMPO oxidized cellulose
Aggregate
Morphology
Crystallinity
Re-dispersibility

ABSTRACT

The applicability of cellulose and its derivatives is greatly depends on their attributes such as aspect ratio, morphology, surface chemistry, crystallinity, as well as their thermal and mechanical properties. However, these attributes can alter according to the utilized raw material, size classifications, extraction techniques, or fibrillation methods. Among these, the effect of raw material particle size on cellulose properties has received limited attention in scientific studies. Therefore, this study aimed to investigate the effect of different particle sizes of spent coffee grounds (SCG) (A: 850–1400 μm, B: 500–850 μm, C: 355–500 μm) on the physicochemical properties of TEMPO-oxidized cellulose (TOC). The freez-dried TOC was characterized in terms of functional groups, morphology, width diameter, crystallinity, carboxyl content, charge density, thermal properties, and re-dispersibility in water. Successful oxidation in all samples was confirmed by the presence of a sodium carboxylate peak in the FTIR spectrum. Higher thermal resistance, carboxyl content, as well as improved physical stability of the re-dispersed suspension were observed in A-TOC sample. Unlike B and C-TOC, A-TOC was favored sample for obtaining fibrillated cellulose with crystallinity of 49.92 %. In contrast, production process significantly damaged the crystalline regions in finer particles and reduced the crystallinity of B and C-TOC to values ranging from 35 to 37 %. In conclusion, finer SCG particles were highly sensitive to reaction conditions and showed high tendency toward dissolution, which make them unsuitable candidates for fiber fabrication. In terms of SCG, only coarse particles (A: 850–1400 μm) were found to be ideal for producing oxidized cellulose fibers.

1. Introduction

Annually, a considerable amounts of food waste are generated throughout the supply chain, from production to distribution and consumption pathways, posing serious environmental, economic, and nutritional challenges. To address these issues, the effective management and valorization of food waste are widely pursued by governments to conserve resources and reduce environmental impact [1].

Spent coffee grounds (SCG) are one of the food waste produced by large-scale coffee manufacturers (instant coffee), as well as coffee shops and restaurants [2]. In 2021 alone, the global production of SCG reached an estimated 18 million wet tonnes [3]. SCG is generally composed of protein (13–17 %), lipids (7–21 %), cellulose (8–15 %), hemicellulose (30–40 %), and lignin (20–30 %) [4]. Its chemical composition, along with high annual and sustainable production [3], makes SCG valuable raw material for the production of

* Corresponding author.
E-mail address: moeenfard@um.ac.ir (M. Moeenfard).

https://doi.org/10.1016/j.heliyon.2025.e41646
Received 29 September 2024; Received in revised form 26 December 2024; Accepted 2 January 2025
Available online 2 January 2025

biogas, oil and biodiesel, plasticizer, bioplastic, compost and fertilizer, adsorbents for pollution remediation, as well as food products (e.g., bakery and meat products) [2]. Furthermore, SCG can be utilized for cellulose extraction and its derivatives, such as cellulose nanocrystals (CNC) [5], cellulose nanospheres (CNS) [6], and cellulose nanofibers (CNF) [7].

Producing cellulose fibers requires advanced mechanical treatments, like high-pressure homogenization, microfluidization, or ultrasonic processing, which effectively disintegrate cellulose bundles into individual fibers [8,9]. However, the efficient fibrillation of cellulose is particularly challenging due to its compact structure, which is reinforced by a network of intra- and intermolecular hydrogen bonds [10]. Alternatively, TEMPO (2,2,6,6tetramethylpiperidinyloxyl)-mediated oxidation can reduce energy demands and facilitate mechanical fibrillation by introducing negative surface charges on fibrils, thereby weakening their interactions through enhanced electrostatic repulsion [11]. This procedure was first proposed by de Nooy et al. [12] and since then, has gained popularity among researchers for its simplicity and ease of functionalization [7,13–15].

Cellulose and its derivatives have been extensively utilized across various fields, including biomedical [16], textile [17], and food applications [18], wastewater treatment [19], as a replacement for synthetic fibers in lightweight polymer composites [20,21]; as well as many other industries [22]. In general, the broad range of applications has driven an increase in natural fiber production, which reached 32.9 million tons globally [23]. However, the practical applications of cellulose fibers and their derivatives depend on their physical and chemical properties, such as morphology, dimensions, aspect ratio, surface chemistry, wettability, crystallinity, as well as thermal and mechanical properties [20,21,24–26]. For example, CNF with higher crystallinity leads to superior thermal stability and lower gas penetration in CNF-based membranes, which are important factors in material science [15]. In alkali-treated *Ficus Macrocarpa* fibers, a combination of higher cellulose content, larger crystalline size, and smaller fiber diameters resulted in significant improvements in thermal stability, tensile strength, and wettability, making the cellulose fibers particularly effective as reinforcements in polymer composites [20]. The integration of fibers with high crystallinity into composite materials likely enhances their mechanical properties, particularly their modulus and stiffness [21]. It has also been shown that higher fiber length correlates with increased viscosity and stronger gel-like elasticity [27], and weaker interfacial stabilization in pickering emulsions [28]. On the other hand, shorter CNFs improve mechanical strength, texture, and oil-binding capacity of oleogels [29]. Moreover, TEMPO-oxidized cellulose nanofibers (TOCNF) with higher carboxylate content reduced the hydrophilicity of coated films by increasing the contact angle [30], led to denser hydrogel structures [31], and sped up drug release from cellulose beads [32]. The aforementioned examples demonstrate that the applications of cellulose fibers are largely determined by their properties, making it essential to tailor these properties to meet specific demands [26].

Consequently, the physicochemical properties of cellulose fibers and their derivatives are influenced by the raw material [15], extraction techniques [33], chemical composition of cellulosic pulp [34], fibrillation methods [8], and other post-treatments [35]. Similarly, the particle size of the raw material is an important factor. Size classification impacts how the raw material behaves during chemical extraction and modification processes, yielding cellulose with distinct chemical composition, dimensions, morphology, crystallinity, and thermal or mechanical characteristics [36], which opens up a range of applications. According to Oluyamo Sunday et al. [36], cellulose extracted from finer wood dust showed higher crystallinity with improved stiffness, rigidity, and strength, resulting in superior mechanical and reinforcing properties. Our previous study [6] demonstrated that the CNS derived from SCG with larger particles exhibited greater diameter, zeta potential, and thermal stability than those obtained from smaller particles [6]. Likewise, the use of smaller CNC ensures better coverage of oil droplets, reduces the mean diameter of emulsion droplets, and ultimately leads to enhanced emulsion stability [37]. As shown by Ratnakumar et al. [38], reducing the particle size of rice straw from 150-250 μm to less than 75 μm improved extraction yield, but resulted in shorter fibers. Alhaji Mohammed et al. [39] demonstrated that finer almond shell particles produced cellulose fibers characterized with higher crystallinity and reduced thermal stability. Research by Adekoya et al. [40] also revealed that the properties of cellulose from *Albizia gummifera* were influenced by particle size, with larger particles yielding 55 % crystallinity compared to 61 % in smaller particles.

To the best of our knowledge, the effect of the particle size of SCG on physicochemical properties of TEMPO-oxidized cellulose (TOC) has not yet been explored. It is well established that different cold and hot coffee beverages are brewed from roasted and ground coffee with varying grind sizes [41]. Therefore, the present study aimed to investigate how the particle sizes of SCG influences the properties of TOC derived from them. To achieve this objective, the oxidized celluloses were characterized based on several parameters, including morphology, carboxyl content, ζ-potential, crystallinity, crystal size, thermal stability, and water re-dispersibility. Since dried samples are more practical for large-scale transportation, this study focused on evaluating all properties of TOC in their dried state. Understanding how the particle size of the raw material affects the properties of the TOC is essential for selecting suitable processing materials and enhancing the material's performance to meet defined objectives.

2. Material and methods

2.1. Materials

Chemicals, including *n*-hexane, sodium hydroxide, sodium hypochlorite (17 %), and hydrochloric acid (37 %), were purchased from Mojallali Company (Iran). TEMPO radical, glacial acetic acid and a dialysis membrane (10 kDa) were obtained from Sigma-Aldrich (Germany). Deionized water with an electrical conductivity of 0.1–0.3 μS was obtained from Betagen (Iran). All compounds were of reagent grade and used as received.

Roasted Robusta coffee beans (100 %, Uganda, medium to high roast) were ground using a home coffee grinder (Taurus, Spain) and sieved into three size fractions: 850–1400 μm (sample A), 500–850 μm (sample B), and 355–500 μm (sample C). The samples were extracted using deionized (DI) water under continuous stirring at 90 ± 2 °C for 20 min. After filtration, the SCGs were oven-dried and

used as the starting material for cellulose extraction.

The fully dried Robusta coffee was also analyzed for its total protein, lipid, ash, and carbohydrate content [6]. Holocellulose content was quantified using the nitric acid-ethanol method with two consecutive extractions, as previously described [42]. Table 1 presents the chemical compositions of the Robusta coffee used in this study.

2.2. Extraction of cellulose

Cellulose was extracted following the procedure described by Shi et al. [43], with slight modifications. Briefly, SCG (sample A, B or C) was first defatted using *n*-hexane in a Soxhlet apparatus. Afterward, 40 g of the defatted material was dispersed in 400 mL NaOH solution (2 mol/L) and stirred at 90 °C for 1 h. After filtration and thorough washing with deionized water, the solid material was bleached using 3 % v/v NaClO solution (acidified to pH 4.5 with glacial acetic acid) at 90 °C for 2 h. After thorough washing with deionized water, the resulting white solid was collected and used in the subsequent oxidation process.

2.3. TEMPO-mediated oxidation of cellulose

Oxidized celluloses were prepared according to a well-established procedure described previously [7,44]. Never dried cellulose (1.0 g of solid content) was suspended in 130 mL of deionized water containing TEMPO (20 mg) and NaBr (0.1 g). Oxidation was initiated by adding 60 mL of NaClO (4–5%) at pH 10-10.5, under constant stirring at room temperature. The pH of the suspension was continuously adjusted with 1 mol/L NaOH solution to maintain a value of approximately 10.3. After 3 h of oxidation, when the pH was stabilized, 20 mL of absolute ethanol was added to terminate the reaction. After centrifugation at 5000 rpm for 5 min, the oxidized cellulose was thoroughly washed with deionized water and dialyzed at 4 °C for about 2 days. A 1.5 % (w/v) aqueous solution of oxidized cellulose was homogenized for 2 min using an ultraturrax (IKA-T25, Germany, 13 mm probe). It was then sonicated with a probe ultrasonic homogenizer (UHP, 400 W, Ultrasonic Technology Development Company, Iran) in alternating 10 s on/off cycles, achieving a total "on" time of 4 min. The resulting TEMPO-oxidized cellulose (TOC) was freeze-dried for subsequent analysis. The step-by-step process for fabricating oxidized cellulose is illustrated in Fig. 1.

2.4. Characterization of TOC

2.4.1. Field emission scanning electron microscopy (FE-SEM)

Morphological characterization of freeze-dried A-, B- and C-TOC was performed using FE-SEM (LMU TESCAN BRNO-Mira 3, Czech Republic) at accelerating voltage of 10 and 20 kV, following the instrument's protocol. Gold sputter-coating was applied to all samples beforehand to improve conductivity.

2.4.2. FTIR analysis

To analyze the chemical functional groups, the samples were mixed with KBr (~1:100, w/w) and pressed into transparent pellets. The FTIR spectra were recorded using an FTIR (Spectrum Two, PerkinElmer, USA) over the scan range of 500–4000 cm^{-1}.

2.4.3. Size distribution and ζ-potential

To determine the ζ-potential of A-, B- and C-TOC (pH 7.5–7.8), never dried TOC samples were diluted in deionized water (~0.5 % w/v) and analyzed in duplicate using a Zetasizer (Nano ZS, Malvern Panalytical, UK) at 25 °C.

The widths of freeze-dried A-, B- and C-TOC samples were calculated by processing FE-SEM images using ImageJ software. A distribution histogram of the data was then generated with OriginPro 2022.

2.4.4. X-ray diffraction measurements (XRD)

The XRD measurements were conducted using a Philips PW1730 system (Philips, Netherlands) at 40 kV and 30 mA. The diffraction angle (2θ) ranged from 5 to 40°, with a scanning rate of 1.5° per min and a step size of 0.05°.

The crystallinity index (*CrI*) was calculated according Eq. (1), where I_{200} represents the maximum intensity of the crystalline cellulose peak at 2θ ~22.5° and I_{am} corresponds to the intensity of amorphous cellulose at the 2θ approximately 18.5° in cellulose I. Crystal sizes were determined according to Scherrer's equation (Eq. (2)) where D is the average crystal size (nm), λ is the X-ray wavelength (1.54059 Å), 0.9 is the Scherrer constant, θ is the diffraction angle for the I_{200} plane in degree, and β is the peak width at half its maximum in radians [14].

$$CrI\ (\%) = \frac{I_{200} - I_{am}}{I_{200}} \times 100 \qquad \text{Equation 1}$$

Table 1
Chemical composition of Robusta coffee (% w/w, dry weight).

Carbohydrate	Lipid	Protein	Ash	Cellulose
76.04 ± 2.80	9.77 ± 1.08	11.84 ± 0.63	2.35 ± 0.49	11.72 ± 1.58

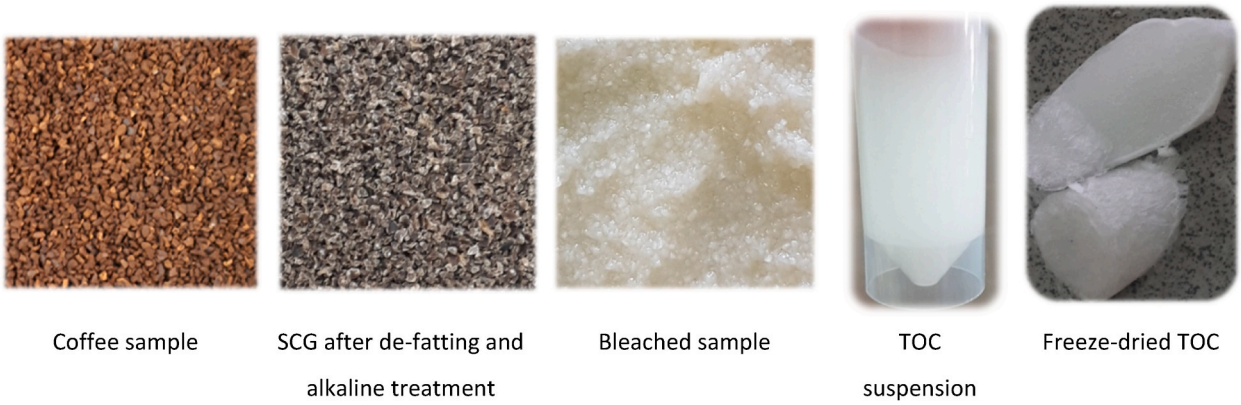

Fig. 1. The process sequence for extraction of TEMPO-oxidized cellulose (TOC) from spent coffee ground (SCG) with particle size of 500–850 μm (sample B).

$$D = \frac{0.9\,\lambda}{\beta \cos\theta} \qquad \text{Equation 2}$$

2.4.5. Carboxyl groups content

The carboxyl group content was determined using a titration method. For this, 50 mg of freeze-dried A-, B-, or C-TOC was soaked in 50 mL of deionized water, treated with an ultraturrax for 1 min, and sonicated for 4 min. The pH was first adjusted to 2.3–2.4 using 0.1 mol/L HCl solution. Titration was then performed with 0.1 mol/L NaOH solution, while monitoring the pH continuously until it reached 10. A plot of pH versus the volume of NaOH titrant was subsequently generated. The titration was conducted at least three times. The carboxyl content was calculated using Eq. (3), following the method of Tanpichai and Wimolmala [45]:

$$C_{COOH} = \frac{C_{NaOH}(v_2 - v_1)}{m} \times 1000 \qquad \text{Equation 3}$$

where C_{COOH} is the carboxyl content of TOC (mmol/g), C_{NaOH} is the concentration of NaOH solution (0.1 mol/L), v_1 and v_2 are the volumes of NaOH solution used at the first and second equilibrium points (mL), respectively, and m is the weight of the sample (g).

2.4.6. Thermogravimetric analysis

The thermal stability of the A-, B-, or C-TOC (5 mg) was determined using a thermal analyzer (Q600, TA Instrument, USA) over a temperature range of 30–500 °C at a heating rate of 10 °C/min under a nitrogen stream.

2.4.7. Re-dispersion of TOC in water

Freeze-dried A-, B-, and C-TOC were dispersed in deionized water (~1.0 % w/v) using an ultraturrax for 1 min, followed by 4 min of sonication in an ice bath. Prolonged processing was avoided to minimize dimensional changes in the oxidized cellulose. Suspension stability was visually assessed over a 12-day period based on the clarity of the supernatant.

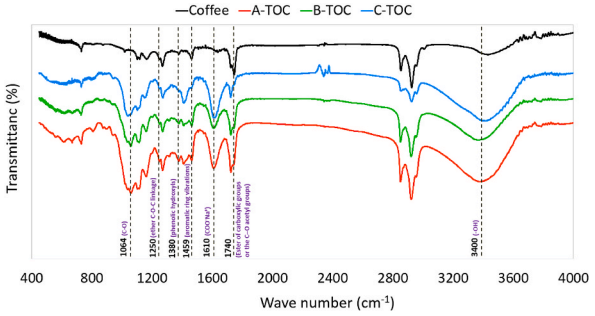

Fig. 2. FTIR spectra of Robusta coffee and resulted A-, B- and C-TOC.

3. Results and discussion

3.1. FTIR analysis of TOC

As shown in Fig. 2, the spectra of the TOCs exhibited a high degree of similarity, suggesting that the chemical structures of the cellulose fibers were not altered by the applied chemical or mechanical treatments to raw materials of different particle sizes. In all spectra, the broad peak within the range of 3300–3600 cm^{-1} is attributed to the stretching vibrations of surface hydroxyl functional groups (-OH), providing evidence of the hydrophilic nature of the cellulose [38]. Distinct spectral differences were identified at 1610 cm^{-1} among A-, B-, C-TOC and SCG, corresponding to the C=O stretching vibrations of the sodium carboxylate group ($COO^{-}Na^{+}$). This peak serves as evidence of the oxidation process in cellulose [29]. The peak at 1064 cm^{-1} is assigned to C–O stretching of the cellulose backbone and can be treated as an internal standard [46]. According to Tang et al. [46], this peak is not influenced by TEMPO-mediated oxidation. The significantly higher intensity of this peak in TOC samples compared to coffee indicates a greater cellulose content in the TOC samples. A peak at 1735-1740 cm^{-1}, associated with ester linkages of carboxylic groups in ferulic and *p*-coumaric acids and/or the C–O stretching of acetyl groups in hemicellulose [9], suggests the likely presence of hemicellulose in A- and B-TOC. As observed, the obtained spectra exhibited a considerable decrease in the intensity of this band in C-TOC. Peaks corresponding to lignin were confirmed by the presence of some bands in the range of 1200–1600 cm^{-1} [47]. For example, the bands at 1250 cm^{-1} (related to the elongation of the ether C-O-C linkage), 1380 cm^{-1} (associated with phenolic hydroxyls) and 1450-1460 cm^{-1} (associated with either aromatic ring vibrations or CH_3 of the acetyl group) [47] indicate that lignin was not entirely removed during the conversion of SCG to TOC. Thus, the presence of impurities in A-, B-, and C-TOC could be roughly inferred. Other studies [45,48] have also confirmed the presence of hemicellulose and lignin in their synthesized cellulose fibers.

It is worth noting that exposing SCG to intensive chemical treatments (suh as using concentrated reagents, prolonged heating, or repeatedly performing lignin and hemicellulose removal processes) can severely damage cellulose fibers, leading to substantial reductions in their yield and dimensions. Moreover, studies have shown that retaining a certain amount of hemicellulose and lignin can facilitate fibrillation during mechanical disintegration [34]. Therefore, in order to minimize damage to the cellulose fibers, the preliminary alkaline and bleaching treatments in this study were limited to a single cycle, leading to only partial removal of lignin and

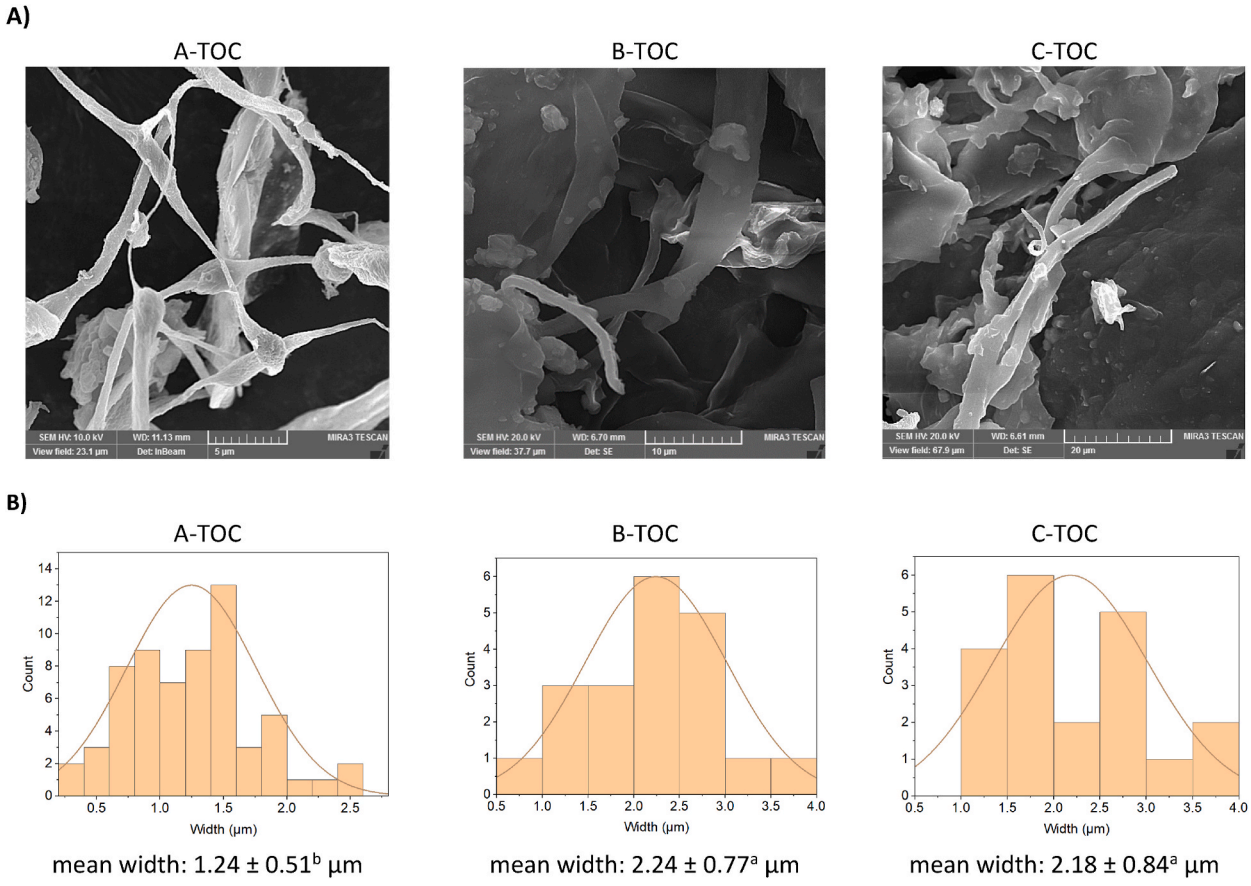

Fig. 3. A) FE-SEM images and, **B)** the mean width of the freeze-dried A-, B- and C-TOC. Means with different letter are significantly different ($p < 0.05$).

hemicellulose.

3.2. Morphology and dimension of TOC

Fig. (3-A) illustrates the changes in the morphology of freeze-dried TOCs with the particle size of the raw material. As it is clearly visible, the fibrous structure of cellulose was more prominent in the A-TOC sample. However, in samples B-TOC and particularly C-TOC, the cellulose fibers were replaced by aggregates and irregular shaped particles. Probably, due to the significant increase in the surface area-to-volume ratio [36], the disordered regions of cellulose in finer particles (B and C) became more chemically accessible and underwent extensive degradation during alkali and bleaching treatments, as well as TEMPO mediated oxidation. This excessive breakdown also rendered the cellulose more vulnerable to subsequent mechanical disintegration.

Enhanced accessibility likely led to the cleavage of shorter oxidized fibers and their release from the bulk material into the suspension [11,46], which were ultimately removed during the washing process. Similarly, fine particles may contribute to the formation of increased amounts of water-soluble polyglucuronates [49], which are subsequently eliminated from the TOC through repeated washing. This process resulted in noticeable reduction in the number of fibers and an increase in irregular structures, as smaller particles are more prone to forming flakes and aggregates during the drying process.

Despite TEMPO oxidation and ultrasonication, the TOCs were not fully individualized, and their dimensions remained within the micron scale. According to Fig. (3-B), the fiber widths increased from 1.24 ± 0.51 μm in A-TOC to approximately 2.18–2.24 μm in B- and C-TOC. While, B- and C-TOC exhibited a broad width distribution, with ~95 % of fibers ranging between 1 and 4 μm, the A-TOC displayed a narrower and more uniform distribution, with ~94 % of micro/nanofibrils widths falling within 0.5–2.5 μm range. The narrower fiber widths observed in A-TOC may be attributed to the retention of some hemicellulose (Section 3.1), which reportedly weakens the hydrogen bonding between cellulose microfibrils, thereby promoting fibrillation. Additionally, the higher carboxyl group content (Table 2) and the resulting electrostatic repulsion might also contribute to enhanced fibrillation observed in A-TOC sample.

In a similar context, it has been reported that residual pectin can effectively inhibit the aggregation of CNF [50]. Similar findings were also reported by Levanič et al. [11] in a study of softwood dissolving pulp (SWDP), where the fiber width increased from 27.71 μm in control-SWDP to approximately 28.71 μm in TEMPO-SWDP after 120 min of oxidation. This change was attributed to the effects of electric charge and electrostatic repulsion.

3.3. Carboxyl content of TOC

Table 2 presents the carboxyl content of re-dispersed TOC suspensions. A notable reduction in carboxyl content was observed from A-TOC to B- and C-TOC. However, the difference between the values for B- and C-TOC (0.64–0.68 mmol/g) was negligible. The lower amount of carboxyl can be explained by three reasons: a) As observed in the FE-SEM images, B- and C-TOC suspensions formed aggregates more effectively. This could hinder the availability of carboxyl ions, as the aggregates resist to cleavage even under mechanical agitation. b) FE-SEM images confirmed a reduced presence of fibers in B- and C-TOC samples, likely due to the dissolution and subsequent removal of shorter oxidized fibers during the washing process. This reduction may decrease the number of carboxylated groups per mass of sample. c) The carboxyl groups associated with residual hemicellulose, as identified through FTIR analysis [50], may also contribute to the overall carboxyl content, which seems to be higher in larger particles.

Similar carboxyl content values have been reported in the literatures for CNFs, ranging from 0.67 to 0.69 mmol/g in *Humulus lupulus* [44], 1.45–1.68 mmol/g in *paulownia fortunei* [14], 1.5 mmol/g in hard wood [51], 1.03 mmol/g in *Olea europaea* pruning residue, 0.77 mmol/g in *Eucalyptus globulus* [52], and 1.9 mmol/g in *Eucalyptus globulus* [33].

3.4. ζ-potential of TOC

The ζ-potential of the re-dispersed suspensions of freeze-dried TOC was also evaluated, with the results presented in Table 2. Only minor differences were observed among the analyzed samples ($p > 0.05$), with ζ-potentials ranging from −18.06 to −22.81 mV. These observations corroborate our earlier findings, demonstrating a direct relation between the carboxyl group content (1.08 mmol/g) and the greater negative charge (−22.81 mV) in A-TOC. It is noteworthy that these results differ significantly from those of never-dried TOC suspensions, which exhibited ζ-potentials ranging from −57.35 to −62.41 mV at a pH of approximately 7.8 (data not shown).

Drying induces various phenomena, including increased concentration, restricted fiber mobility, and enhanced surface exposure and interactions, all of which can lead to aggregates formation [53]. This aggregation may explain the low ζ-potentials observed in samples A-, B-, and C-TOC. Additionally, as described by Silva et al. [53], fibers may undergo further fragmentation into smaller pieces

Table 2
Carboxyl content, ζ-potential, crystallinity index (*CrI*) and crystal size of the studied samples *.

Samples	A-TOC	B-TOC	C-TOC
Carboxyl content (mmol/g)	1.08 ± 0.18^{a}	0.68 ± 0.07^{b}	0.64 ± 0.11^{b}
ζ-potential (mV)	-22.81 ± 3.69^{a}	-18.06 ± 2.18^{a}	-19.38 ± 1.13^{a}
Crystallinity index (%)	49.92 ± 1.52^{a}	35.11 ± 0.42^{b}	37.24 ± 1.76^{b}
Crystal size (nm)	3.48	3.65	3.21

* Means within rows with different letter are significantly different ($p < 0.05$).

after a drying/redispersion cycle due to the effects high shear forces. These smaller pieces can adhere to fibril surfaces, creating more compact aggregates [53] which, in turn, result in reduced ζ-potentials. Since B- and C-TOC contain fewer and shorter fibers, they are more susceptible to surface coverage by fine particles, providing an additional explanation for their lower ζ-potentials compare to A-TOC. Furthermore, as previously noted, the carboxyl groups of residual hemicellulose (Section 3.1) may also contribute to the value of ζ-potential [50].

Intriguingly, although the carboxyl content varied significantly (0.64–1.08 mmol/g), the observed differences in ζ-potential among the samples were negligible. This result is consistent with the findings of Okita et al. [54], who investigated the correlation between carboxyl content and ζ-potential in TEMPO-oxidized cellulose nanofibers (TOCNFs) derived from various biomass sources. Despite substantial variation in carboxyl content (0.52–1.65 mmol/g), the ζ-potentials of TOCNFs remained nearly identical (~−75 mV). This observation suggests that ζ-potential values are influenced by the surface density of dissociated carboxyl groups rather than the total carboxyl content [54].

3.5. XRD analysis and crystallinity index

The XRD diffractograms of the TOC samples are shown in Fig. (4-A). Accordingly, the A-TOC exhibited the characteristic pattern of

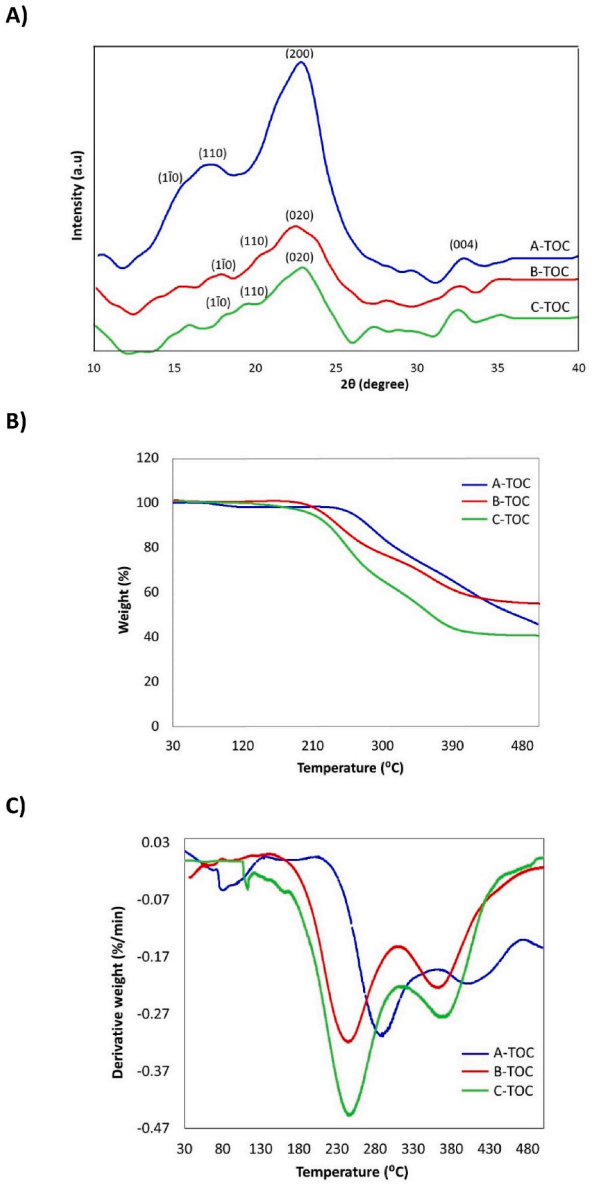

Fig. 4. A) XRD diffractograms, **B)** TGA curves and **C)** DTG curves of the A-, B- and C-TOC.

cellulose I, as indicated by the absence of a doublet signal at 2θ ~22.8° [15]. The peak at approximately 2θ ~22.5° corresponds to the diffraction of the (200) crystalline plane [50], while the peaks at around 14–15°, 17–18°, and 32–33° are attributed to the (1$\bar{1}$0), (110), and (004) lattice planes of cellulose I, respectively [53,55]. According to Gong et al. [55], the diffraction peaks at 2θ around 12°, 20°, 22° are associated with the (1$\bar{1}$0), (110), and (020) planes in cellulose II, respectively. This suggests that the B- and C-TOC samples are a mixture of cellulose types I and II. The observed peak intensities were most prominent in A-TOC and significantly declined in B- and C-TOC, indicating that the microfibrillar morphology and crystal structure of cellulose were progressively damaged from A-to C-TOC. Consistent with the XRD diffractograms, the calculated *CrI* values (Table 2) revealed a decreasing trend from A-TOC (49.92 %) to B (35.11 %) and C-TOC (37.24 %). The low *CrI* values in B- and C-TOC are likely due to significant damage to the crystalline regions of cellulose, caused by the combined effects of TEMPO-mediated oxidation and mechanical disintegration [56]. Notably, the larger

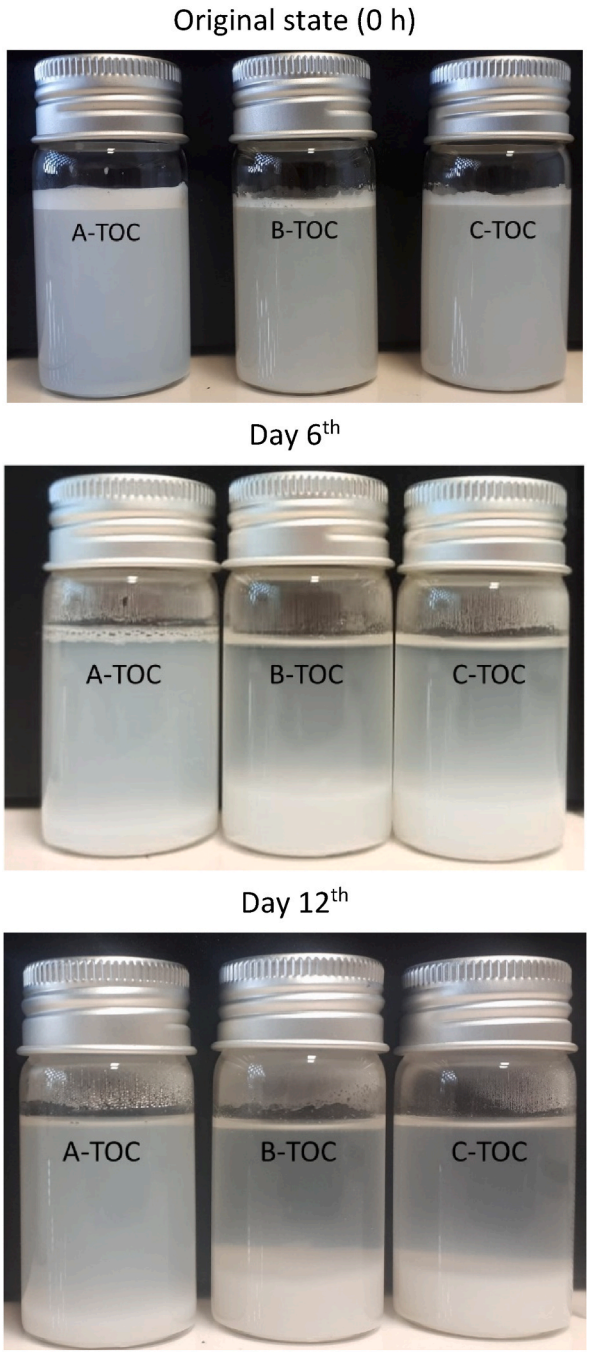

Fig. 5. Visual observation of re-dispersed freeze-dried A-, B- and C-TOC in water.

surface area of smaller raw materials makes them more susceptible to oxidation by TEMPO and also other chemical agents.

Moreover, as noted by Isogai [57], $COO^{-}Na^{+}$ groups are densely, position-selectively formed on the surfaces of crystalline cellulose microfibrils. Therefore, the observed decrease in diffraction intensity at $2\theta = 22.0–22.8^{\circ}$ and the subsequent reduction in *CrI* can also be explained also by the following reasons: a) the accelerated dissolution of the highly oxidized crystalline regions in B- and C-TOC, and b) the weaker hydrogen bonds between cellulose chains in B- and C-TOC, due to a lower amount of hydroxyl groups, which disrupts the regular structure of cellulose molecules [58]. Contrary to our observations, other researchers [39,40] found that the *CrI* of cellulose increased as the particle size of the raw material decreased, likely due to the efficient removal of non-cellulosic components.

Despite the decrease in *CrI*, the crystal size remained unaffected by the particle size of the raw material, staying within the range of 3.21–3.65 nm. The literature reports various crystal sizes for TOCNFs, including an average crystal size of 4.2 nm from SCG [7], 4.3–4.5 nm from waste hop stems [44], 4.5–6.2 nm from cotton, 3.5–4.1 nm from hardwood, and 5.4–6.2 nm from bacterial cellulose [54].

3.6. Thermogravimetric analysis (TGA) of TOC

Fig. (4-B) and (4-C) show the thermogravimetric analysis (TGA) curves and derivative thermogravimetric (DTG) curves, respectively, within the temperature range of 30–500 °C. Since the samples were dried before TGA analysis, the weight loss below 100 °C, primarily attributed to the evaporation of adsorbed water, was negligible. A-TOC exhibited an onset of thermal decomposition (T_{onset}) at approximately 215 °C, which was significantly higher than the T_{onset} observed for B- and C-TOC, both at approximately 160 °C (Fig. 4-C). After 220 °C, two distinct stages of degradation and mass loss were observed in all samples. For A-TOC, the first maximum thermal decomposition temperature (T_{max1}) occurred at approximately 290 °C, while the second (T_{max2}) was observed at around 404 °C. Compared to A-TOC, the degradation temperatures for B- and C-TOC shifted to lower values. T_{max1} occurred at 246 °C and 250 °C, while T_{max2} was observed at 365 °C and 353 °C for B- and C-TOC, respectively.

It has been reported that the T_{max1} represents the thermal decomposition of the sodium carboxylate units, while the T_{max2} corresponds to the degradation of the remaining cellulose backbones, along with any residual hemicellulose and lignin [44,59]. Although higher charge density and the presence of sodium carboxylate groups typically make fibers more prone to thermal degradation [43,60], A-TOC exhibited the highest thermal stability, likely due to its higher degree of crystallinity and longer fibrous structure. As mentioned in section (3.6), the major crystalline regions of B- and C-TOC were substantially damaged during the production process. More importantly, the decomposition temperature is strongly correlated with the number of reducing end groups. Therefore, the reduction in fiber length and content, as observed in the B- and C-TOC samples, leads to a higher density of reducing end groups per unit mass, which act as initiation sites for degradation [60].

3.7. Re-dispersibility of TOC

TOC re-dispersibility in deionized water was evaluated by monitoring the extent of TOC precipitation and the clarity of the supernatant, with the results presented in Fig. 5. All suspensions exhibited noticeable precipitation within the first 3 h. However, a visual assessment revealed that A-TOC settled less and remained more stable over 12 days of incubation at room temperature, compared to B- and C-TOC.

It is well documented that various morphological characteristics of fibers are significantly influenced by both the type and conditions of the drying process. Drying hinders redispersion by intensifying hydrogen bonding and promoting the formation of high-density aggregates, both of which negatively affect dispersion stability [50,53]. Our FE-SEM images further confirmed that, unlike the compact flakes and short fibers observed in the B- and C-TOC samples, A-TOC exhibits a network-like structure. This structural feature enhances the hydrophilic nature of A-TOC and improves its interaction with water molecules [61]. Moreover, the superior re-dispersibility of A-TOC can be attributed to its higher carboxyl content and electrostatic repulsion [14], both of which enhance colloidal stability in the re-dispersed suspension. As also noted by Saito et al. [51], TEMPO-oxidized cellulose with a carboxylate content below 1.5 mmol/g exhibited a tendency to settle in water, whereas those with a carboxylate content of 1.5 mmol/g or higher formed stable suspensions.

4. Conclusion

This study investigated the physicochemical properties of TEMPO-oxidized cellulose (TOC) extracted from spent coffee grounds (SCG) with different particle sizes classification. A-, B- and C-TOC were produced through a series of steps, including dewaxing, delignification, bleaching, TEMPO-mediated oxidation, mechanical fibrillation, and freeze-drying. In general, the particle size of the raw material affected all parameters except for crystal size and the ζ-potential of the dried samples. The success of selective oxidation in all samples was confirmed by the presence of the sodium carboxylate peak at 1610 cm^{-1}. Morphological observations from FE-SEM images revealed that A-TOC formed a network-like structure of cellulose bundles. In contrast, B- and C-TOC were characterized by shorter, and wider oxidized fibers, along with abundant self-aggregates. XRD analysis confirmed that A-TOC exhibited greater crystallinity than B- and C-TOC, suggesting that the crystalline regions in B- and C-TOC were significantly damaged during the preparation. According to thermogravimetric analysis, A-TOC demonstrated superior thermal stability compared to the other samples. Additionally, the presence of more aggregates and a lower negative charge of B- and C-TOC samples contributed to their reduced suspension stability. In contrast, the fibrous structure of A-TOC made its suspension more stable. This study highlights the significant impact of particle size of raw material on the physical and chemical properties of TOC, emphasizing the importance of selecting appropriate raw

material dimensions to tailor cellulose fibers for specific applications. In conclusion, it is crucial to note that the optimal particle size may vary depending on the type of raw material and the production approach. Therefore, it is strongly recommended that researchers consider these factors before producing oxidized cellulose fibers.

CRediT authorship contribution statement

Hooriyeh Rahmani Khoshk: Methodology, Investigation. **Marzieh Moeenfard:** Writing – review & editing, Writing – original draft, Validation, Supervision, Resources, Project administration, Funding acquisition, Formal analysis, Conceptualization.

Data availability statement

- All data generated or analyzed during this study are included in this published article.

Funding sources

This work was supported by the Ferdowsi University of Mashhad [grant number: 3/59235].

Declaration of competing interest

The authors declare that they have no known competing financial interests or personal relationships that could have appeared to influence the work reported in this paper.

References

[1] A. Sarker, R. Ahmmed, S.M. Ahsan, J. Rana, M.K. Ghosh, R. Nandi, A comprehensive review of food waste valorization for the sustainable management of global food waste, Sustainable Food Technology 2 (1) (2024) 48–69.
[2] A.S. Franca, L.S. Oliveira, Potential uses of spent coffee grounds in the food industry, Foods 11 (14) (2022).
[3] D. Kim, J. Cha, C. Lee, Enhanced methane production with co-feeding spent coffee grounds using spare capacity of existing anaerobic food waste digesters, Sci. Rep. 14 (1) (2024) 4472.
[4] A.S. Bomfim, D.M. Oliveira, H.J. Voorwald, K.C. Benini, M.-J. Dumont, D. Rodrigue, Valorization of spent coffee grounds as precursors for biopolymers and composite production, Polymers 14 (3) (2022).
[5] S. Deb Dutta, D.K. Patel, K. Ganguly, K.-T. Lim, Isolation and characterization of cellulose nanocrystals from coffee grounds for tissue engineering, Mater. Lett. 287 (2021) 129311.
[6] M. Ostadi Moghadam, M. Moeenfard, How does particle size of spent coffee ground affect the physicochemical properties of isolated cellulose nanosphere? Results in Chemistry 10 (2024) 101683.
[7] N. Kanai, T. Honda, N. Yoshihara, T. Oyama, A. Naito, K. Ueda, I. Kawamura, Structural characterization of cellulose nanofibers isolated from spent coffee grounds and their composite films with poly(vinyl alcohol): a new non-wood source, Cellulose 27 (9) (2020) 5017–5028.
[8] J. Zeng, F. Hu, Z. Cheng, B. Wang, K. Chen, Isolation and rheological characterization of cellulose nanofibrils (cnfs) produced by microfluidic homogenization, ball-milling, grinding and refining, Cellulose 28 (6) (2021) 3389–3408.
[9] M. Dilamian, B. Noroozi, A combined homogenization-high intensity ultrasonication process for individualizaion of cellulose micro-nano fibers from rice straw, Cellulose 26 (10) (2019) 5831–5849.
[10] B. Mazela, W. Perdoch, B. Peplińska, M. Zieliński, Influence of chemical pre-treatments and ultrasonication on the dimensions and appearance of cellulose fibers, Materials 13 (2020).
[11] J. Levanič, V.P. Šenk, P. Nadrah, I. Poljanšek, P. Oven, A. Haapala, Analyzing tempo-oxidized cellulose fiber morphology: new insights into optimization of the oxidation process and nanocellulose dispersion quality, ACS Sustain. Chem. Eng. 8 (48) (2020) 17752–17762.
[12] A.E.J. de Nooy, A.C. Besemer, H. van Bekkum, Highly selective nitroxyl radical-mediated oxidation of primary alcohol groups in water-soluble glucans, Carbohydr. Res. 269 (1) (1995) 89–98.
[13] L.M. Hillscher, M.V. Höfler, T. Gutmann, C. Lux, K.U. Clerkin, G. Schwall, K. Villforth, S. Schabel, M. Biesalski, Influence of tempo-oxidation on pulp fiber chemistry, morphology and mechanical paper sheet properties, Cellulose 31 (5) (2024) 3067–3082.
[14] E. Kaffashsaie, H. Yousefi, T. Nishino, T. Matsumoto, M. Mashkour, M. Madhoushi, H. Kawaguchi, Direct conversion of raw wood to tempo-oxidized cellulose nanofibers, Carbohydrate Polymers 262 (2021) 117938.
[15] A.W. Pratama, B. Piluharto, M. Mahardika, N. Widiastuti, A. Firmanda, M.N.F. Norrrahim, Comparative study of oxidized cellulose nanofibrils properties from diverse sources via tempo-mediated oxidation, Case Studies in Chemical and Environmental Engineering 10 (2024) 100823.
[16] J. Yusuf, S.M. Sapuan, M.A. Ansari, V.U. Siddiqui, T. Jamal, R.A. Ilyas, M.R. Hassan, Exploring nanocellulose frontiers: a comprehensive review of its extraction, properties, and pioneering applications in the automotive and biomedical industries, Int. J. Biol. Macromol. 255 (2024) 128121.
[17] H. Zheng, X. Li, L. Liu, C. Bai, B. Liu, H. Liao, M. Yan, F. Liu, P. Han, H. Zhang, J. He, Preparation of nanofiber core-spun yarn based on cellulose nanowhiskers/quaternary ammonium salts nanocomposites for efficient and durable antibacterial textiles, Compos. Commun. 36 (2022) 101388.
[18] Z. Li, S. Anankanbil, J.N. Pedersen, M. Nadzieja, Z. Guo, Nanocellulose fractionated from tempo-mediated oxidation of cellulose as an energy-free ingredient for stabilizing pickering emulsion, Biochem. Eng. J. 191 (2023) 108795.
[19] R. Sharma, P.C. Nath, Y.K. Mohanta, B. Bhunia, B. Mishra, M. Sharma, S. Suri, M. Bhaswant, P.K. Nayak, K. Sridhar, Recent advances in cellulose-based sustainable materials for wastewater treatment: an overview, Int. J. Biol. Macromol. 256 (2024) 128517.
[20] J. Tengsuthiwat, V. A, V. R, Y.G. T. G, S.M. Rangappa, S. Siengchin, Characterization of novel natural cellulose fiber from ficus macrocarpa bark for lightweight structural composite application and its effect on chemical treatment, Heliyon 10 (9) (2024) e00938.
[21] R. Srisuk, L. Techawinyutham, A. Vinod, S. Mavinkere Rangappa, S. Siengchin, Agro-waste from bambusa flexuosa stem fibers: a sustainable and green material for lightweight polymer composites, J. Build. Eng. 73 (2023) 106674.
[22] H. Yang, H. Zheng, Y. Duan, T. Xu, H. Xie, H. Du, C. Si, Nanocellulose-graphene composites: preparation and applications in flexible electronics, Int. J. Biol. Macromol. 253 (2023) 126903.
[23] E. Syafri, V. Ayyappan, V. Raghunathan, S.M. Rangappa, S. Siengchin, Editor's corner: green materials-the advancements and applications of natural fibers, Journal of Fibers and Polymer Composites 2 (2) (2023) 168–173.
[24] S. Huang, X. Liu, C. Chang, Y. Wang, Recent developments and prospective food-related applications of cellulose nanocrystals: a review, Cellulose 27 (6) (2020) 2991–3011.

[25] J.-S. Tang, C.-T. Kuo, Y.-C. Liao, Transparent biodegradable composite plastic packaging film from tempo-oxidized cellulose nanofibers, Int. J. Biol. Macromol. 260 (2024) 129502.
[26] T. Aziz, A. Farid, F. Haq, M. Kiran, A. Ullah, K. Zhang, C. Li, S. Ghazanfar, H. Sun, R. Ullah, A. Ali, M. Muzammal, M. Shah, N. Akhtar, S. Selim, N. Hagagy, M. Samy, S.K. Al Jaouni, A review on the modification of cellulose and its applications, Polymers 14 (2022).
[27] T. Yuan, J. Zeng, B. Wang, Z. Cheng, K. Chen, Cellulosic fiber: mechanical fibrillation-morphology-rheology relationships, Cellulose 28 (12) (2021) 7651–7662.
[28] Pickering emulsion stabilized by cellulosic fibers: morphological properties-interfacial stabilization-rheological behavior relationships, Carbohydrate Polymers 269 (2021) 118339.
[29] Y. Zou, Y. Tian, B. Zhao, J. Li, J. Luo, J. Sheng, X. Li, Effects of cellulose diameter on the formation and rheological properties of edible walnut oleogels structured by cellulose nanofiber, Food Hydrocolloids 154 (2024) 110149.
[30] G. Rodionova, Ø. Eriksen, Ø. Gregersen, Tempo-oxidized cellulose nanofiber films: effect of surface morphology on water resistance, Cellulose 19 (4) (2012) 1115–1123.
[31] X. Li, P. He, R. Ma, C. Dong, Y. Lv, L. Dai, Modulation of composite hydrogel consisting of tempo-oxidized cellulose nanofibers and cationic guar gum, Int. J. Biol. Macromol. 241 (2023) 124483.
[32] F. Xie, P. De Wever, P. Fardim, G. Van den Mooter, Tempo-oxidized cellulose beads as potential ph-responsive carriers for site-specific drug delivery in the gastrointestinal tract, Molecules 26 (2021).
[33] H. Xu, J.L. Sanchez-Salvador, A. Balea, A. Blanco, C. Negro, Optimization of reagent consumption in tempo-mediated oxidation of eucalyptus cellulose to obtain cellulose nanofibers, Cellulose 29 (12) (2022) 6611–6627.
[34] C. Lin, Q. Deng, Y. Hu, L. Huang, Y. Ni, S. Cao, X. Ma, Effects of hemicellulose content on tempo-mediated selective oxidation, and the properties of films prepared from bleached chemical pulp, Cellulose 27 (2) (2020) 1043–1054.
[35] Y. Yoshikawa, K. Yamato, A. Ishida, Y. Yoshida, Y. Kumamoto, A. Isogai, Amidation of carboxy groups in tempo-oxidized cellulose for improving surface hydrophobization and thermal stability of tempo-cncs, Carbohydrate Polymers (2024) 122654.
[36] S. Oluyamo Sunday, A. Adekoya Mathew, in: P. Alejandro Rodríguez, E.E.M. María (Eds.), Influence of Size Classifications on the Structural and Solid-State Characterization of Cellulose Materials, Cellulose, IntechOpen, Rijeka, 2019. Ch. 3.
[37] X. Li, J. Li, J. Gong, Y. Kuang, L. Mo, T. Song, Cellulose nanocrystals (cncs) with different crystalline allomorph for oil in water pickering emulsions, Carbohydrate Polymers 183 (2018) 303–310.
[38] A. Ratnakumar, A.M.P.B. Samarasekara, D.A.S. Amarasinghe, L. Karunanayake, The influence of particle size on the extraction of cellulose nanofibers using chemical-ultrasonic process, Mater. Today: Proc. 45 (2022) 5714–5719.
[39] M. Alhaji Mohammed, W.J. Basirun, N.M.M. Abd Rahman, N. Salleh, The effect of particle size of almond shell powders, temperature and time on the extraction of cellulose, J. Nat. Fibers 19 (13) (2022) 5577–5587.
[40] M.A. Adekoya, S. Liu, S.S. Oluyamo, O.T. Oyeleye, R.T. Ogundare, Influence of size classifications on the crystallinity index of albizia gummifera cellulose, Heliyon 8 (12) (2022) e12019.
[41] M. Petracco, in: R.J. Clarke, O.G. Vitzthum (Eds.), Technology Iv: Beverage Preparation: Brewing Trends for the New Millennium," *Coffee: Recent Developments*, Blackwell Sience, UK, 2001, pp. 140–164.
[42] Q. Chen, S. Xiao, S.Q. Shi, L. Cai, Isolation of cellulose from poplar wood by nitric acid-ethanol treatment and its effect on the quality of films cast from ionic liquid, Bioresources 13 (4) (2018) 8943–8955.
[43] C. Shi, Y. Chen, Z. Yu, S. Li, H. Chan, S. Sun, G. Chen, M. He, J. Tian, Sustainable and superhydrophobic spent coffee ground-derived holocellulose nanofibers foam for continuous oil/water separation, Sustainable Materials and Technologies 28 (2021) e00277.
[44] N. Kanai, K. Nishimura, S. Umetani, Y. Saito, H. Saito, T. Oyama, I. Kawamura, Upcycling of waste hop stems into cellulose nanofibers: isolation and structural characterization, ACS Agricultural Science & Technology 1 (4) (2021) 347–354.
[45] S. Tanpichai, E. Wimolmala, Facile single-step preparation of cellulose nanofibers by tempo-mediated oxidation and their nanocomposites, J. Nat. Fibers 19 (15) (2022) 10094–10110.
[46] Z. Tang, W. Li, X. Lin, H. Xiao, Q. Miao, L. Huang, L. Chen, H. Wu, Tempo-oxidized cellulose with high degree of oxidation, Polymers 9 (2017).
[47] N.Y. Abu-Thabit, A.A. Judeh, A.S. Hakeem, A. Ul-Hamid, Y. Umar, A. Ahmad, Isolation and characterization of microcrystalline cellulose from date seeds (phoenix dactylifera l.), Int. J. Biol. Macromol. 155 (2020) 730–739.
[48] I.P. Mahendra, W.B. Tamrin, I. H, M. J.A, Thermal and morphology properties of cellulose nanofiber from tempo-oxidized lower part of empty fruit bunches (lefb) 17 (1) (2019) 526–536.
[49] A. Isogai, Y. Zhou, Diverse nanocelluloses prepared from tempo-oxidized wood cellulose fibers: nanonetworks, nanofibers, and nanocrystals, Curr. Opin. Solid State Mater. Sci. 23 (2) (2019) 101–106.
[50] W. Yu, Y. Yi, H. Wang, Y. Yang, C. Xing, L. Zeng, J. Tang, Z. Tan, Effects of residual pectin composition and content on the properties of cellulose nanofibrils from ramie fibers, Carbohydrate Polymers 298 (2022) 120112.
[51] T. Saito, S. Kimura, Y. Nishiyama, A. Isogai, Cellulose nanofibers prepared by tempo-mediated oxidation of native cellulose, Biomacromolecules 8 (8) (2007) 2485–2491.
[52] Ú. Fillat, B. Wicklein, R. Martín-Sampedro, D. Ibarra, E. Ruiz-Hitzky, C. Valencia, A. Sarrión, E. Castro, M.E. Eugenio, Assessing cellulose nanofiber production from olive tree pruning residue, Carbohydrate Polymers 179 (2018) 252–261.
[53] L.E. Silva, A.d.A. dos Santos, L. Torres, Z. McCaffrey, A. Klamczynski, G. Glenn, A.R.d. Sena Neto, D. Wood, T. Williams, W. Orts, R.A.P. Damásio, G.H.D. Tonoli, Redispersion and structural change evaluation of dried microfibrillated cellulose, Carbohydrate Polymers 252 (2021) 117165.
[54] Y. Okita, T. Saito, A. Isogai, Entire surface oxidation of various cellulose microfibrils by tempo-mediated oxidation, Biomacromolecules 11 (6) (2010) 1696–1700.
[55] J. Gong, J. Li, J. Xu, Z. Xiang, L. Mo, Research on cellulose nanocrystals produced from cellulose sources with various polymorphs, RSC Adv. 7 (53) (2017) 33486–33493.
[56] S. Wang, X. Wang, W. Liu, L. Zhang, H. Ouyang, Q. Hou, K. Fan, J. Li, P. Liu, X. Liu, Fabricating cellulose nanofibril from licorice residues and its cellulose composite incorporated with natural nanoparticles, Carbohydrate Polymers 229 (2020) 115464.
[57] A. Isogai, Emerging nanocellulose technologies: recent developments, Adv. Mater. 33 (28) (2021) 2000630.
[58] X. Kang, P. Sun, S. Kuga, C. Wang, Y. Zhao, M. Wu, Y. Huang, Thin cellulose nanofiber from corncob cellulose and its performance in transparent nanopaper, ACS Sustain. Chem. Eng. 5 (3) (2017) 2529–2534.
[59] R. Qu, M. Tang, Y. Wang, D. Li, L. Wang, Tempo-oxidized cellulose fibers from wheat straw: effect of ultrasonic pretreatment and concentration on structure and rheological properties of suspensions, Carbohydrate Polymers 255 (2021) 117386.
[60] O.M. Vanderfleet, M.S. Reid, J. Bras, L. Heux, J. Godoy-Vargas, M.K.R. Panga, E.D. Cranston, Insight into thermal stability of cellulose nanocrystals from new hydrolysis methods with acid blends, Cellulose 26 (1) (2019) 507–528.
[61] A. Isogai, *Development of completely dispersed cellulose nanofibers*, Proceedings of the Japan Academy, Series B, Physical and biological sciences 94 (4) (2018) 161–179.